1 Response to Anonymous Referee #2

Author response: Thank you for your detailed comments on our manuscript. We believe we have addressed each request. Below, we provide a point-by-point reply to each comment. Please note that the other reviewer requested a comprehensive instrumental and measurement uncertainty analysis. Please see the attached supplementary document that describes the Monte Carlo radiative transfer simulations that we performed for this purpose.

This study presents attenuation flux coefficients using spectral irradiance measurements of bare glacial ice in western Greenland. These coefficients are compared with theory and other data sets. The authors conclude that attenuation is enhanced due to a semi-granular near-surface ice layer and by light absorbing impurities at their measurement location. As attenuation flux coefficients for glacial ice are scarce, the data set presented in this study is therefore an important addition for the scientific community. The manuscript is generally well written with clear figures. The following issues should be addressed before publication:

General comments:

1) The title and part of the introduction (line 81-91) looked a bit strange to me. I got the impression that a significant part of the study is a about the ICEsat satellite, while it is only briefly discussed in Sect. 4.3. Therefore, I would suggest to shorten the title and leave out the ICEsat part and shorten the part of the introduction about ICEsat to take away the confusion.

Author reply: As requested, we shortened the title and removed the ICESat part. We moved the ICESat paragraph from the introduction to the discussion where it provides an example for how our dataset can be used (c.f. Deems et al., 2013; Smith et al., 2018).

2) The Kangerlussuaq region is well known to have a high LAP concentration (e.g., Wientjes et al., 2011; Tedstone et al., 2020). Therefore, it is not surprising that impurities impact the results. The authors, however, state on various occasions in the manuscript that there might be LAPs involved, almost like it is a new finding (e.g., line 331-333: "Comparison with the spectral coefficient for pure ice (Figure 4c) suggests the discrepancy we find is likely due to LAPs present in the measured volume, which appear to disproportionately enhance energy absorption near the ice surface" or on line 385-386: "This suggest light absorbing particles enhance visible light absorption and reduce optical penetration depth at our field site"). I think that the manuscript would benefit if more literature is used to determine if the results are in agreement with the observed LAP concentration for this region.

Author reply: We did not measure LAP concentration directly; therefore, we were cautious in noting that we infer LAP influence. Our intention is not to suggest absorption by LAPs is surprising. However, it is also important to acknowledge that prior studies reported on albedo and/or reflectance, whereas the results referenced here relate to transmittance at >12 cm depth below the ice surface and therefore provide additional context regarding light absorption by LAPs within the ice volume, rather than on or very near the ice surface.

3) The authors state that no asymptotic flux attenuation coefficients are available for glacial ice (e.g., line 72-73), but Ackermann et al. (2006) (which is cited in this manuscript) reported absorption coefficients for glacial ice in Antarctica. Although it is true that Ackermann et al. (2006) measured deep glacial ice in Antarctica while the authors measured bare glacial ice in Greenland, for some cases it compares relatively well with the results presented in the manuscript, as you have shown in Fig. 9. Furthermore, Ackermann et al. (2006) show the absorption coefficient for 532 nm (Fig. 16 of that paper), which does not seem to

not match the statement on line 89-91. I would like these issues discussed on the relevant places in this study or an explanation why the authors think it is not comparable (For example, on line 72-73, line 89-91, line 226-229, line 305-307, Sect. 4.3, Fig. 4b, Fig. 9).

Author reply: We removed the claim "first" everywhere to avoid confusion. We acknowledge the need to distinguish our results from those of Ackermann et al. (2006). There are two main distinctions: 1) compressed glacial ice at >800 m depth has no granular structure, and 2) absorptivity of compressed glacial ice at >800 m depth is controlled by factors that are only partly relevant to the ice sheet surface (dust concentrations from past millennia). The Ackermann et al. (2006) results demonstrate that scattering at >800 m depth is mainly controlled by clathrates, indicating that air bubbles are also of little importance. An earlier study, closely related to the Ackerman study, concludes: "Scattering … at ice–ice boundaries … will be of minor importance" (Price and Bergström, 1997). Consequently, the two main factors that control light scattering near the ice sheet surface (granularity and air bubbles) are of minor importance to the light scattering results presented by Ackermann et al. (2006).

Although we agree that Fig. 16 of Ackermann et al. (2006) compares relatively well with our results, it is important to acknowledge that this is at least in part incidental, and different physical mechanisms are at play in both cases. It is not our intention to suggest that Ackermann's results are irrelevant to our study or that our study is incomparable to that study. Rather, the underlying physical mechanisms that control light attenuation are different in both cases. As such, we have removed claims of "first" throughout the paper and we added additional context for the difference between our study and the Ackermann et al. (2006) study in the relevant discussion.

4) Figure 4b should be replaced by Fig. 9, as Fig 4b seems redundant. Furthermore, a discussion in more detail about Fig. 9 is desirable. On one hand it shows that the results of this study are in agreement with AMANDA 1755 m, and support the claim that impurities are an important factor (which is mentioned on various places in the manuscript, like on line 226-229 or line 282-283). However, on the other hand it shows that the difference with the pure-ice estimate of Picard et al. 2016 is very small. This is confusing for me. I also think that Fig. 4a and Fig. 8 can be merged.

Author reply: We removed Fig. 4 and we point to Fig. 8 and 9 where we previously pointed to Fig. 4, as requested. We added a new paragraph that concludes the Discussion section focused on Fig. 9.

5) Most Figures are barely introduced in the manuscript, while a highly detailed description is provided in the caption. I would suggest to move some of the caption to the main text.

Author reply: We addressed this throughout the manuscript, as requested.

6) It would have been better for the χ term that is introduced in Sect. 2.5 to be wavelength dependent, as attenuation in the surface layer strongly depends on wavelength (e.g., Fig. 6 and 7 of (Grenfell and Maykut, 1977)). This maybe could explain the increasing difference with wavelength for the 12 cm depth fit in Fig. 5c. As the differences are still rather small, I do not think that it is necessary to adjust the results to a wavelength dependent χ, but I think that the manuscript would benefit if the authors state the uncertainty that arises because of this choice. Also, I do not understand line 195-197. Isn't χ now practically the same as i0 due to the spectral integration?

Author reply: We originally included the spectrally averaged value because large-scale models often need a single value for the visible and a single value for the infrared, or one single broadband

value (Briegleb and Light, 2007; Liston and Winther, 2005). We now report spectral $\chi(\lambda)$ values in addition to the average value, as requested by another reviewer.

The reason we distinguish χ and i_o is because i_o is defined in such a way that it partitions the absorbed solar flux, or the net solar flux divergence, whereas we use χ to partition the downward flux. Grenfell and Maykut (1977) use their albedo measurements and modeling to extend their albedo and extinction coefficients across the solar spectrum and thereby to calculate the net flux divergence. Overall, our main goal with this part of the paper is to communicate the idea that a surface scattering layer is present on the ice sheet, and that this concept is well-developed in the sea ice literature but is conspicuously absent from the glaciological literature. To that end, we felt that a single χ value was sufficient to communicate that message.

7) Figure 7, lines 268 – 275 and Sect. 3.5, except for line 285-287, should be moved to the methods.

Author reply: We moved these sections and Fig. 7 to the methods, as requested.

8) Use the abbreviation 'Fig.' when referring to a figure in running text, unless it is at the beginning of the sentence.

Author reply: This has been corrected throughout the manuscript, as requested.

Minor comments:
Line 65: Change "size > wavelength" to "size larger than wavelength"

Author reply: This has been corrected, as requested.

Line 66-69: Add references to this statement.

Author reply: We added the following references to this statement:

Brandt, R. E. and Warren, S. G.: Solar-heating rates and temperature profiles in Antarctic snow and ice, Journal of Glaciology, 39(131), 99–110, doi:10.3189/S0022143000015756, 1993.

Liston, G. E., Bruland, O., Elvehøy, H. and Sand, K.: Below-surface ice melt on the coastal Antarctic ice sheet, Journal of Glaciology, 45(150), 273–285, doi:10.3189/002214399793377130, 1999.

Wiscombe, W. J. and Warren, S. G.: A Model for the Spectral Albedo of Snow. I: Pure Snow, J. Atmos. Sci., 37(12), 2712–2733, doi:10.1175/1520-0469(1980)037<2712:AMFTSA>2.0.CO;2, 1980.

For all equations: Use punctuation at the end of the equation, as the equation is part of a sentence.

Author reply: This has been corrected, as requested.

Line 148-149: What do you mean with "Solid ice-equivalent values?"

Author reply: "Solid ice-equivalent values" refers to normalization of the k_{att} values by the ratio of solid ice density to measured (sample) density:

$$k_{\mathrm{i}} = \frac{\rho_{\mathrm{i}}}{\rho} k_{\mathrm{att}}$$

where ρ is measured ice density, ρ_{i} is solid ice density (917 kg m^{-3}), k_{i} is k_{att} in units of (inverse) "solid-ice equivalent thickness" [m^{-1}] and k_{att} is in units of (inverse) in-situ ice thickness.

Line 154: g is usually assumed to be independent of wavelength. Also call it the asymmetry factor and define the single-scattering albedo.

Author reply: We now call it the asymmetry factor and we defined the single scattering albedo, as requested. For completeness, we retained the wavelength dependence of g.

Eq 5: Are you sure that Schuster, 1905 is the right reference for this equation? Libois et al. (2013) and Tuzet et al. (2019, cited in this manuscript) describe it relatively well. They also use the Delta-Eddington method, which should be mentioned in the manuscript.

Author reply: The equation we use is derived equivalently from the Eddington approximation or the two-stream derivation given in Bohren, (1987). Schuster, (1905) is usually credited with the asymptotic two-stream solution (Mishchenko, 2013). We cite Tuzet et al. (2019) and Libois et al. (2013) in the manuscript.

Fig. 2.: Please change "Relative irradiance" to "transmittance" and add the units for the standard deviation.

Author reply: We changed "relative irradiance" to "transmittance" in the figure caption and we added the units for standard deviation, as requested.

Fig. 3: Do the authors have any idea why k_att becomes increasingly smaller and very small around 850-900 nm, which does not seem to be in agreement with Warren et al. 2006? I know that in the manuscript it is stated that beyond 700 nm the flux is small and the results become less reliable, but it seems to be odd.

Author reply: The values beyond ~700 nm are inaccurate. We show them to help the reader understand why we restrict our k_{att} values to the range 350–700 nm, whereas transmittance was measured to 900 nm (and is plotted in this range in Fig. 2c).

Line 216: Define the albedo, as e.g. the surface reflectivity of solar radiation .

Author reply: We added a definition for albedo and explained how we calculate it and how we use it.

The text reads: "The ice surface albedo was estimated as the ratio of the 2 m background upwelling spectral irradiance to the downwelling spectral irradiance. These irradiance data were smoothed with the same 1 nm interpolation filter described [for the in-ice irradiance measurements]. The ice surface albedo is presented in Sect. 4 to qualitatively discuss the in-ice irradiance measurements and the $k_{\mathrm{att}}(\lambda)$ estimates."

Line 218: Please use more recent references, e.g. Gardner and Sharp (2010), and/or He and Flanner (2020).

Author reply: We added both of these references. Thank you for alerting us to the review by He and Flanner (2020), it was helpful.

Line 230: Add more references.

Author reply: Line 230 in the discussion paper is a comment that grain size dominates absorption beyond ~530 nm. Line 229 is a comment that LAPs dominate absorption at shorter wavelengths. We are not sure which of these two comments this request is aimed at, but we added the following references that address both comments (He et al., 2017; Libois et al., 2013, 2014):

He, C., Takano, Y., Liou, K.-N., Yang, P., Li, Q. and Chen, F.: Impact of Snow Grain Shape and Black Carbon–Snow Internal Mixing on Snow Optical Properties: Parameterizations for Climate Models, J. Climate, 30(24), 10019–10036, doi:10.1175/JCLI-D-17-0300.1, 2017.

Libois, Q., Picard, G., France, J. L., Arnaud, L., Dumont, M., Carmagnola, C. M. and King, M. D.: Influence of grain shape on light penetration in snow, The Cryosphere, 7(6), 1803–1818, doi:10.5194/tc-7-1803-2013, 2013.

Libois, Q., Picard, G., Dumont, M., Arnaud, L., Sergent, C., Pougatch, E., Sudul, M. and Vial, D.: Experimental determination of the absorption enhancement parameter of snow, Journal of Glaciology, 60(222), 714–724, doi:10.3189/2014JoG14J015, 2014.

Line 241. Do the authors mean Eq. 17 instead of Eq. 16 of Warren et al. (2006)?

Author reply: Yes, thank you, we corrected this.

Fig.6b: Please put k_att(0-12 cm) / k_att on the y-axis and remove the legend.

Author reply: We have made these corrections, as requested.

Line 268: I assume the authors mean with "The field measurements" your observations, and not from Grenfell and Maykut (1977)? Please clarify.

Author reply: Yes, we are referring to our measurements. We clarified this in the revised text.

Line 287: "omega > 800 nm". 800 nm does not make sense, as omega is defined in this manuscript as the single-scattering albedo.

Author reply: This typo has been corrected. The revised text reads: "the maximum difference found was 0.2% for values of ω at wavelengths greater than 800 nm."

Line 323-324: "The comparison demonstrates the tremendous variation in k_att values". The term 'tremendous' is a bit overexaggerated. Besides, the differences are not that large if the absorption coefficient is compared to glacial ice or pure ice (Fig. 9).

Author reply: We revised the text as follows: "The comparison demonstrates that k_{att} values vary by >1 order of magnitude at visible wavelengths due to differences in ice structure and composition"

Line 374: Change “to modelling light attenuation in glacier ice” to “to modelling light attenuation in near-surface glacier ice”.

Author reply: We added “near-surface”, as requested.

Line 394-397: This is a bit vague, please reformulate.

Author reply: We removed this sentence at the request of another reviewer and replaced it with a summary of the scattering and absorption coefficient values that we quantify.

Bibliography (reviewer):

Tedstone, A. J., Cook, J. M., Williamson, C. J., Hofer, S., McCutcheon, J., Irvine- Fynn, T., Gribbin, T. and Tranter, M.: Algal growth and weathering crust state drive variability in western Greenland Ice Sheet ice albedo, The Cryosphere, 14, 521-538, https://doi.org/10.5194/tc-14-521-2020, 2020

Wientjes, I. G. M., Van de Wal, R. S. W., Reichart, G. J., Sluijs, A. and Oerlemans, J.: Dust from the dark region in the western ablation zone of the Greenland ice sheet, The Cryosphere, 5, 589-601, https://doi.org/10.5194/tc-5-589-2011, 2011.

Libois, Q., Picard, G., France, J. L., Arnaud, L., Dumont, M., Carmagnola, C. M., and King, M. D.: Influence of grain shape on light penetration in snow, Cryosphere, 7, 1803–1818, https://doi.org/10.5194/tc-7-1803-2013, 2013.

Gardner, A. S. and Sharp, M. J.: A review of snow and ice albedo and the development of a new physically based broadband albedo parameterization, Journal of Geophysical Research: Earth Surface, 115, https://doi.org/10.1029/2009JF001444, 2010.

He, C. and Flanner, M.: Snow Albedo and Radiative Transfer: Theory, Modeling, and Parameterization, pp. 67–133, Springer International Publishing, Cham, https://doi.org/10.1007/978-3-030-38696-2_3, 2020.

Bibliography (response):

Briegleb, B. P.: Delta-Eddington approximation for solar radiation in the NCAR community climate model, J. Geophys. Res., 97(DBohren, C. F.: Multiple scattering of light and some of its observable consequences, American Journal of Physics, 55(6), 524–533, doi:10.1119/1.15109, 1987.

Briegleb, B. P. and Light, B.: A Delta-Eddington Mutiple Scattering Parameterization for Solar Radiation in the Sea Ice Component of the Community Climate System Model, Technical Note, National Center for Atmospheric Research, Boulder, Colorado. [online] Available from: http://dx.doi.org/10.5065/D6B27S71 (Accessed 18 February 2019), 2007.

Deems, J. S., Painter, T. H. and Finnegan, D. C.: Lidar measurement of snow depth: a review, Journal of Glaciology, 59(215), 467–479, doi:10.3189/2013JoG12J154, 2013.

Grenfell, T. C. and Maykut, G. A.: The Optical Properties of Ice and Snow in the Arctic Basin*, Journal of Glaciology, 18(80), 445–463, doi:10.3189/S0022143000021122, 1977.

He, C., Takano, Y., Liou, K.-N., Yang, P., Li, Q. and Chen, F.: Impact of Snow Grain Shape and Black Carbon–Snow Internal Mixing on Snow Optical Properties: Parameterizations for Climate Models, J. Climate, 30(24), 10019–10036, doi:10.1175/JCLI-D-17-0300.1, 2017.

Libois, Q., Picard, G., France, J. L., Arnaud, L., Dumont, M., Carmagnola, C. M. and King, M. D.: Influence of grain shape on light penetration in snow, The Cryosphere, 7(6), 1803–1818, doi:10.5194/tc-7-1803-2013, 2013.

Libois, Q., Picard, G., Dumont, M., Arnaud, L., Sergent, C., Pougatch, E., Sudul, M. and Vial, D.: Experimental determination of the absorption enhancement parameter of snow, Journal of Glaciology, 60(222), 714–724, doi:10.3189/2014JoG14J015, 2014.

Liston, G. E. and Winther, J.-G.: Antarctic Surface and Subsurface Snow and Ice Melt Fluxes, J. Climate, 18(10), 1469–1481, doi:10.1175/JCLI3344.1, 2005.

Mishchenko, M. I.: 125 years of radiative transfer: Enduring triumphs and persisting misconceptions, pp. 11–18, Dahlem Cube, Free University, Berlin., 2013.

Price, P. B. and Bergström, L.: Optical properties of deep ice at the South Pole: scattering, Appl. Opt., AO, 36(18), 4181–4194, doi:10.1364/AO.36.004181, 1997.

Schuster, A.: Radiation through a foggy atmosphere, The Astrophysical Journal, XX1(1), 1–22, 1905.

Smith, B. E., Gardner, A., Schneider, A. and Flanner, M.: Modeling biases in laser-altimetry measurements caused by scattering of green light in snow, Remote Sensing of Environment, 215, 398–410, doi:10.1016/j.rse.2018.06.012, 2018.

7), 7603, doi:10.1029/92JD00291, 1992.

Deems, J. S., Painter, T. H. and Finnegan, D. C.: Lidar measurement of snow depth: a review, Journal of Glaciology, 59(215), 467–479, doi:10.3189/2013JoG12J154, 2013.

Liston, G. E. and Winther, J.-G.: Antarctic Surface and Subsurface Snow and Ice Melt Fluxes, J. Climate, 18(10), 1469–1481, doi:10.1175/JCLI3344.1, 2005.

Smith, B. E., Gardner, A., Schneider, A. and Flanner, M.: Modeling biases in laser-altimetry measurements caused by scattering of green light in snow, Remote Sensing of Environment, 215, 398–410, doi:10.1016/j.rse.2018.06.012, 2018.

2 New datasets

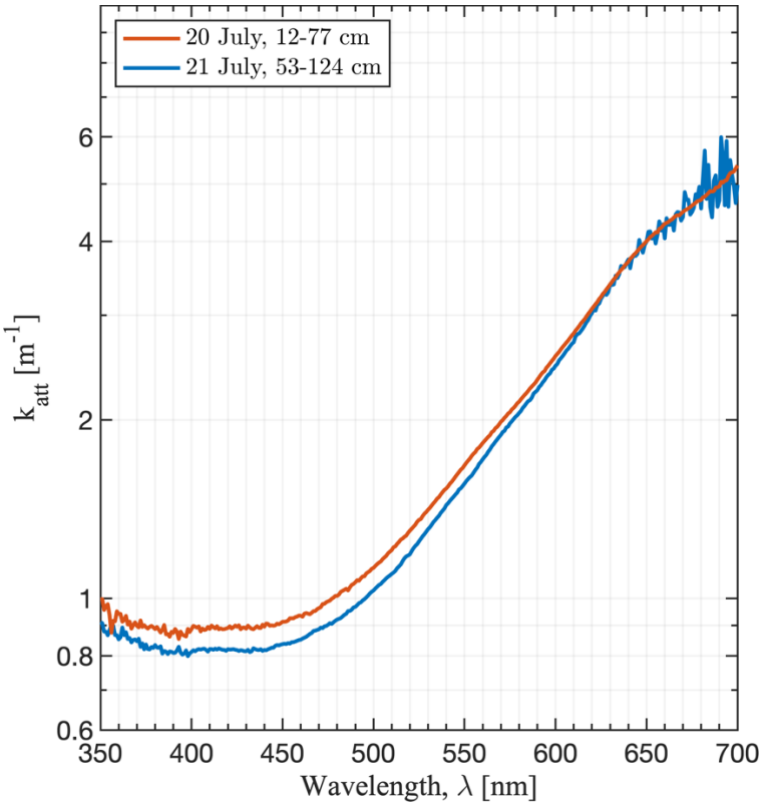

Fig. 1: k_{att} spectra calculated with in-ice irradiance collected on 20 July at depths between 12–77 cm below the ice surface and on 21 July at depths between 53–124 cm below the ice surface. The higher attenuation in the 12–77 cm depth region is consistent with the expectation that impurities have a larger impact on visible light attenuation nearer the ice surface. The close agreement in the 600–700 nm region is consistent with the expectation that ice absorption dominates attenuation in the near infrared. The noise in the 21 July spectrum at longer wavelengths is due to the lower light levels at those depths.

3 Dark light sensitivity

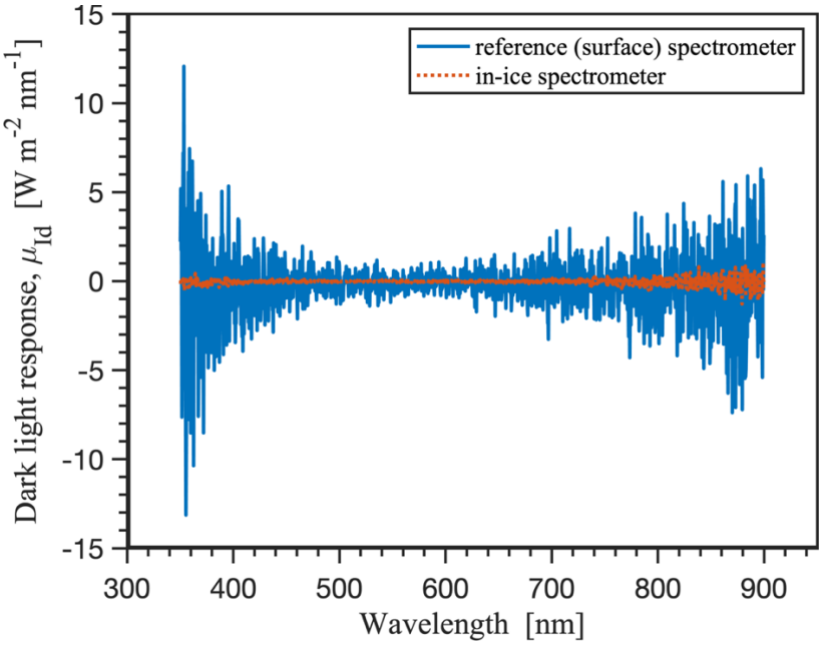

Fig. 2: Measured values of dark-light sensitivity collected with the reference spectrometer that was used to measure downwelling irradiance at 2 m height above the ice surface and with the spectrometer that was used to measure in-ice irradiance. The Ocean View software requires that a measurement of dark light is made prior to each absolute irradiance measurement, and automatically removes the dark light from the measured irradiance. The values shown in this figure represent the residual dark-light sensitivity that remained after the automated software correction. The dark light spectra shown here is subtracted from the irradiance measurements prior to fitting our experimental k_{att} values. Comparison of k_{att} computed with and without this dark-light correction is shown in Fig. 3.

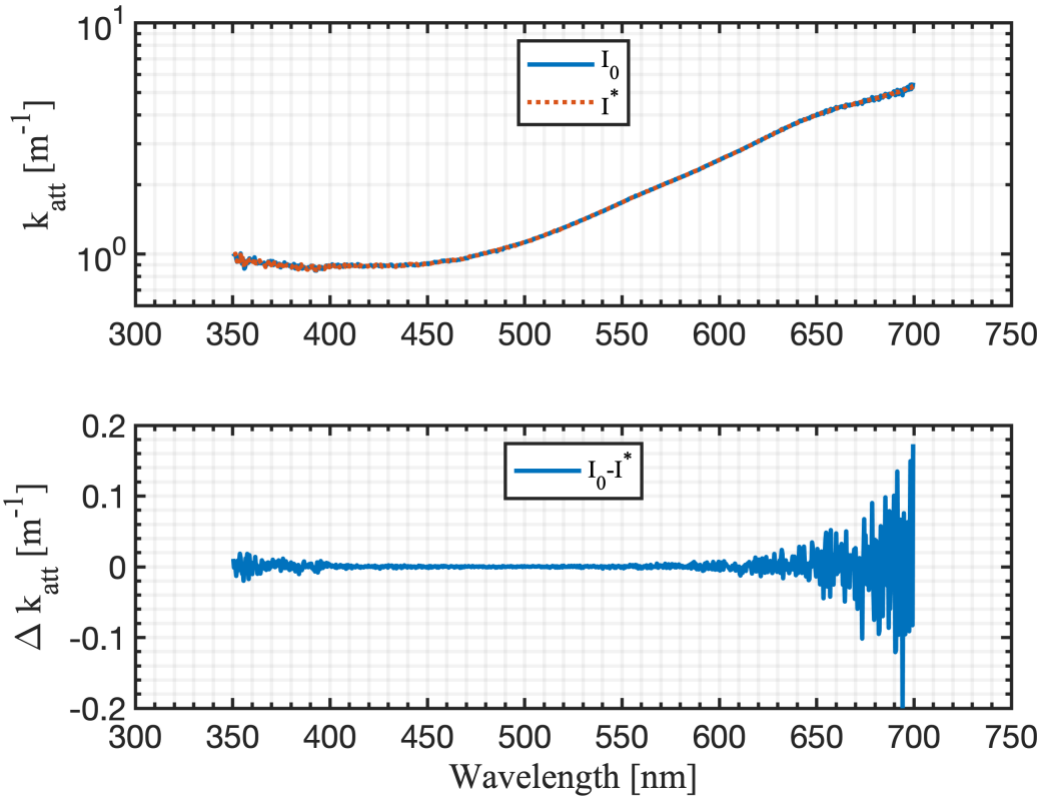

Fig. 3: (a) k_{att} spectra with (I*) and without (I_0) subtracting the dark-light response spectra shown in Fig. 2. (b) the difference between the two spectra in (a), which is used as an estimate of uncertainty due to dark light response ε_D.

4 Statistical variations in the high frequency measurements

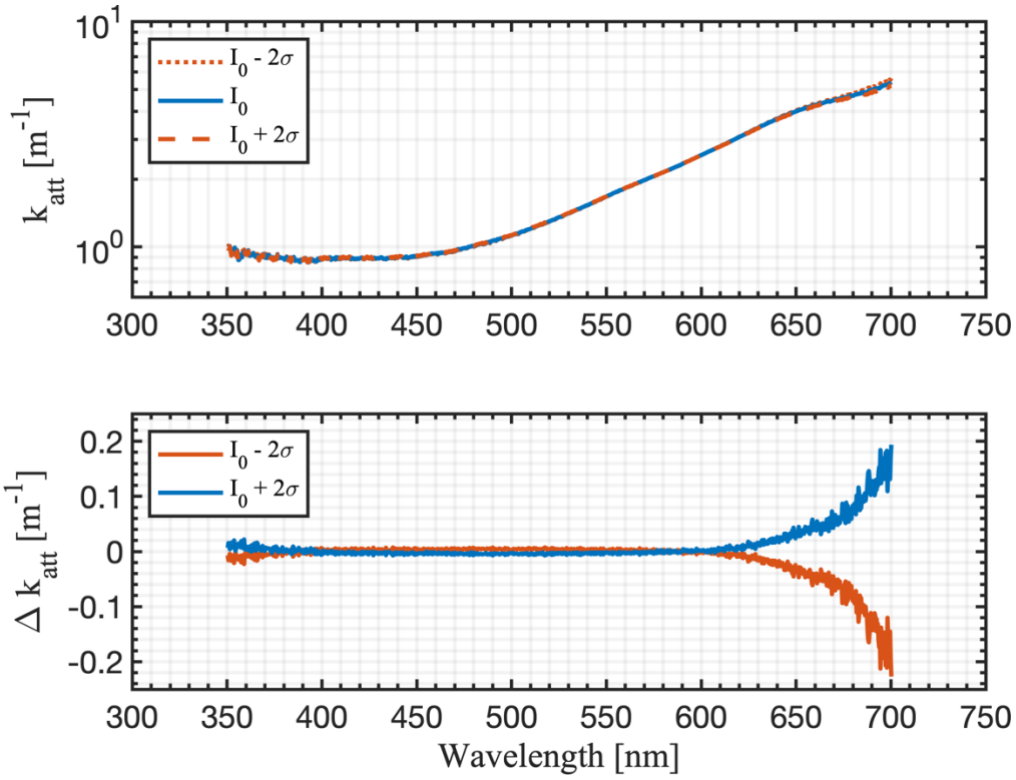

Fig. 4: (a) k_{att} spectra calculated by adding and subtracting two standard deviations in the high-frequency in-ice irradiance data at each depth from the mean value at each depth and re-calculating k_{att} with these modified irradiance values. (b) The difference between the two spectra in (a), which is used as an estimate of uncertainty due to high frequency variability in the irradiance measurements, $\varepsilon_{2\sigma}$.

S1 Monte Carlo radiative transfer model

The Monte Carlo method solves the radiative transfer equation (RTE) by simulating large ensembles of photon events represented by random samples from probability density functions (Ertürk and Howell, 2017). In this study and others, the Monte Carlo method is used to quantify relative uncertainties in imperfect optical measurements that are intractable with analytical or numerical solutions to the RTE (Gordon, 1985). We developed a Monte Carlo radiative transfer model to estimate the effect of detector interference on our irradiance measurements. The model closely follows methods developed to simulate light propagation in biological tissue, ocean waters, and sea ice (Leathers et al., 2004; Light et al., 2003; Wang et al., 1995). A general description of the model and particular modifications for this investigation are described below.

S1.1 Probability functions for optical properties

The fundamental ingredients of this and other Monte Carlo radiative transfer models are the inherent optical properties k, ω, and g (see Sect. 2.3 of the main), the geometric boundary conditions, and the probabilistic rules that govern the system. The cumulative probability of occurrence for an event x, with probability density function $\mathrm{p}(\mathrm{x})$, is:

$$\mathrm{P}(\mathrm{x}) = \int_{-\infty}^{\mathrm{x}} \mathrm{p}(\mathrm{x})\mathrm{dx}, \quad 0 \leq \mathrm{P}(\mathrm{x}) \leq 1. \tag{1}$$

To solve for x, the left-hand-side (LHS) of (1) is replaced with a random number:

$$\mathrm{P}(\mathrm{x}) = q \tag{2}$$

where q is from the uniform distribution over [0,1]. The right-hand-side (RHS) lower limit of integration $-\infty$ is replaced with an appropriate limit (e.g., 0) and analytic or empirical expressions for $\mathrm{p}(\mathrm{x})$ are specified.

In this study, x represents optical path length, scattering direction, and photon survival probability. Closed-form expressions for each of these terms are given in the following sections.

S1.1.1 Optical path length

The probability density function for the optical path length l [m^{-1}] is given by the e-folding length:

$$\mathrm{p}(l) = \mathrm{e}^{-l}, \qquad l \geq 0 \tag{3}$$

with the cumulative distribution function:

$$\mathrm{P}(l) = \int_0^l \mathrm{e}^{-l'}\mathrm{d}l' = 1 - \mathrm{e}^{-l}. \tag{4}$$

From Eq. (2), $q = 1 - \mathrm{e}^{-l}$ and therefore:

$$l = -\ln q\,, \qquad 0 \leq 1. \tag{5}$$

In this study, q is generated with the MATLAB function rand.

The photon transport length [m] is the optical path length scaled by the extinction coefficient:

$$\mathrm{s} = l/\sigma_\mathrm{e} \tag{6}$$

where:

$$\sigma_\mathrm{e} = \sigma_\mathrm{s} + \sigma_\mathrm{a} \tag{7}$$

is the single-scattering extinction coefficient, σ_s [m^{-1}] is the scattering coefficient, and σ_a [m^{-1}] is the absorption coefficient.

S1.1.2 Scattering phase function

The probability density function for a scattering phase function with azimuthal symmetry is:

$$\mathrm{p}(\theta_\mathrm{s}) = 2\pi\tilde{\beta}(\theta_\mathrm{s}) \sin\theta \tag{8}$$

where $\tilde{\beta}(\theta_\mathrm{s})$ is the probability that a photon will scatter at polar angle θ_s. We specify $\tilde{\beta}(\theta_\mathrm{s})$ with the Henyey-Greenstein scattering phase function, which is appropriate for strongly forward scattering by ice grains and air bubbles (Light et al., 2003):

$$\tilde{\beta}(\mathrm{g}, \theta_\mathrm{s}) = \frac{1}{4\pi} \frac{1 - \mathrm{g}^2}{(1 + \mathrm{g}^2 - 2\mathrm{g}\cos\theta_\mathrm{s})^{\frac{3}{2}}}, \qquad -1 < \mathrm{g} < 1. \tag{9}$$

where $\mathrm{g} = 0$ reduces Eq. 9 to isotropic scattering and $\mathrm{g} \to 1$ is strongly forward scattering. In this study, $\mathrm{g} = 0.86$, as given by Mullen & Warren (1988) from Mie theory calculations for scattering by air bubbles in ice.

From Eq. (1):

$$\mathrm{P}(\theta_\mathrm{s}) = -\frac{1 - \mathrm{g}^2}{2} \int_0^{\theta_\mathrm{s}} \frac{\sin\theta_\mathrm{s}'}{(1 + \mathrm{g}^2 - 2\mathrm{g}\cos\theta_\mathrm{s}')^{\frac{3}{2}}} \mathrm{d}\theta_\mathrm{s}' = q \tag{10}$$

which evaluates to:

$$q = \frac{1 - \mathrm{g}^2}{2\mathrm{g}} \left[\frac{1}{1 - \mathrm{g}} - \frac{1}{\sqrt{1 + \mathrm{g}^2 - 2\mathrm{g}\cos\theta_\mathrm{s}}} \right] \tag{11}$$

yielding the scattering angle:

$$\cos\theta_s = \frac{1}{2g}\left[1 + g^2 - \left(\frac{1 - g^2}{1 - g + 2gq}\right)^2\right], \qquad g \neq 0;\ 0 \leq \theta_s \leq \pi/2. \tag{12}$$

The probability density function for scattering azimuth angle ϕ_s in a spherical coordinate system with azimuthal symmetry is $1/2\pi$. From Eq. (1):

$$P(\phi_s) = \frac{\phi_s}{2\pi}, \qquad 0 \leq \phi_s \leq 2\pi \tag{13}$$

and from Eq. (2):

$$\phi_s = 2\pi q. \tag{14}$$

S1.1.3 Photon termination

Monte Carlo simulations are computationally expensive. To improve computational performance, photons are treated as packets of photons with initial weight $w = 1$. At each interaction, photons are scattered and absorbed according to their respective statistical probabilities, parameterized by σ_s and σ_a. Accordingly, at each interaction the weight is updated as:

$$w = (1 - \overline{\omega}) \cdot w \tag{15}$$

where:

$$\overline{\omega} = \sigma_s/\sigma_e \tag{16}$$

is the single-scattering albedo [-]. Each $1 - \overline{\omega}$ reduction in photon packet weight is proportional to the probability of an individual photon absorption event. After many interactions, if w drops below a very small value it contributes very little to the solution. The so-called "Russian roulette" technique is used to improve computational performance, where photon packet weights below a specified threshold $w < w_{min}$ are increased in proportion to a survival probability function and are re-released into the medium, or otherwise terminated:

$$w = \begin{cases} m \cdot w, & q \leq 1/m \\ 0, & q > 1/m \end{cases} \tag{17}$$

where $1/m$ is the probability of photon survival and q is a random number as previously defined. This technique conserves energy and is unbiased (Wang et al., 1995). In this study, $w_{min} = 10^{-5}$ and $m = 10$.

At each interaction, the absorbed fraction $\overline{\omega} \cdot w$ is scored into an absorption array in a cylindrical coordinate system that is used to compute observable quantities of absorption and photon fluence. If a photon packet exits the medium, it is scored into a transmittance or reflectance array in an azimuthally independent spherical coordinate system that is used to compute observable quantities of irradiance, radiant intensity, and power. These scoring systems follow the definitions in Wang et al. (1995) Eq. 4.1–4.32.

The preceding sections describe the fundamental processes of photon transport, scattering direction, and survival probability. Similar probability density functions that describe the detector rod interference are described next.

S1.2 Monte Carlo experiment

The detector rod interference is estimated with a "backward" Monte Carlo (BMC) simulation, which simulates photon trajectories starting from the detector backward to the target (Leathers et al., 2004; Light et al., 2003). Here, the target is the ice surface. The simulation domain is a 3-dimensional ice slab with one boundary, the ice surface, and otherwise infinite horizontal and vertical extent. A cylinder with dimensions identical to the detector rod is placed at positions identical to the measurement depths reported in this paper, and photon packets are released from the irradiance sensor ("remote cosine receptor") located on the detector rod (Fig. 5).

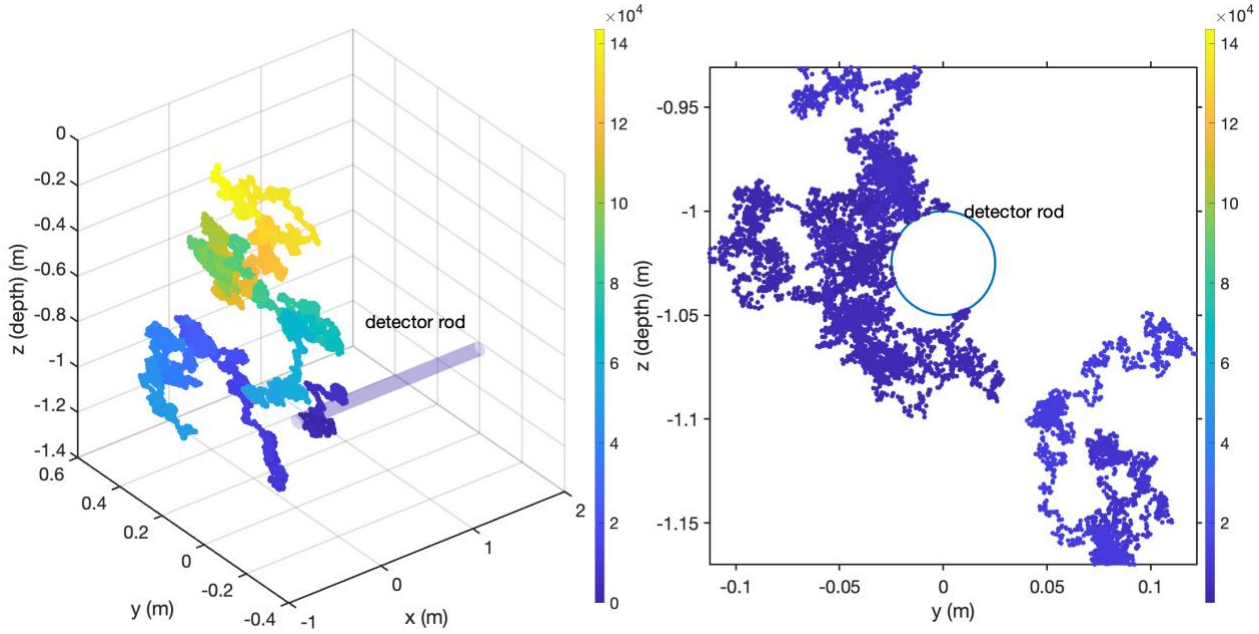

Fig. 5: Example Monte Carlo photon tracking simulation from model output used in this study, with interference by cylindrical detector rod. (a) ~14,000 random photon interactions are traced within a 3-dimensional ice volume. The cylindrical object represents the detector rod, here inserted at 1 m below the ice surface. The photon packet is released from the position of the irradiance sensor ("remote cosine receptor") located on the rod and traced backward to the ice surface ("backward Monte Carlo"). (b) Magnified view of the detector rod in the y-z plane shows photon packets scattering off of the rod. The color-bar represents the number of cumulative interactions experienced by this photon packet.

As described above, each interaction within the ice volume is defined by absorption and scattering of the photon by ice. Absorption reduces the photon energy density by an amount $1 - \overline{\omega}_{\mathrm{ice}}$. Scattering redirects the photon trajectory according to the Henyey-Greenstein scattering phase function with asymmetry

parameter g and transport distance l. Photon interactions with the detector rod require additional specifications that are described next.

S1.2.1 Source function for cosine detector

The scattering phase function for an irradiance sensor with a cosine response is:

$$\tilde{\beta}(\theta) = \frac{\cos\theta}{\pi}, \qquad 0 \le \theta \le \frac{\pi}{2} \tag{18}$$

with probability density function:

$$p(\theta) = 2\pi\tilde{\beta}(\theta)\sin\theta \tag{19}$$

and cumulative distribution function:

$$P(\theta) = 2\int_0^{\theta} \cos\theta' \sin\theta' \, d\theta' = q\,. \tag{20}$$

Substituting $\mu = \cos(\theta)$ the scattering angle is:

$$\cos\theta = \sqrt{1-q}. \tag{21}$$

For a forward Monte Carlo simulation, Eq. 21 gives the probability of photon receipt by an irradiance sensor with an ideal cosine response. For a BMC simulation, the form of Equation 21 that gives the initial launch trajectory of photons from the irradiance sensor surface is:

$$\cos\theta = -\sqrt{q}. \tag{22}$$

In reality, irradiance sensors do not have an ideal cosine response to radiance. In this experiment, the non-ideal cosine response of the irradiance sensor is estimated by replacing Eq. 22 with uniform sampling from an empirical probability density function derived from laboratory measurements of the cosine receptor angular response function provided by Ocean Optics (Fig. 6). The source azimuth angle ϕ is determined with Eq. (14).

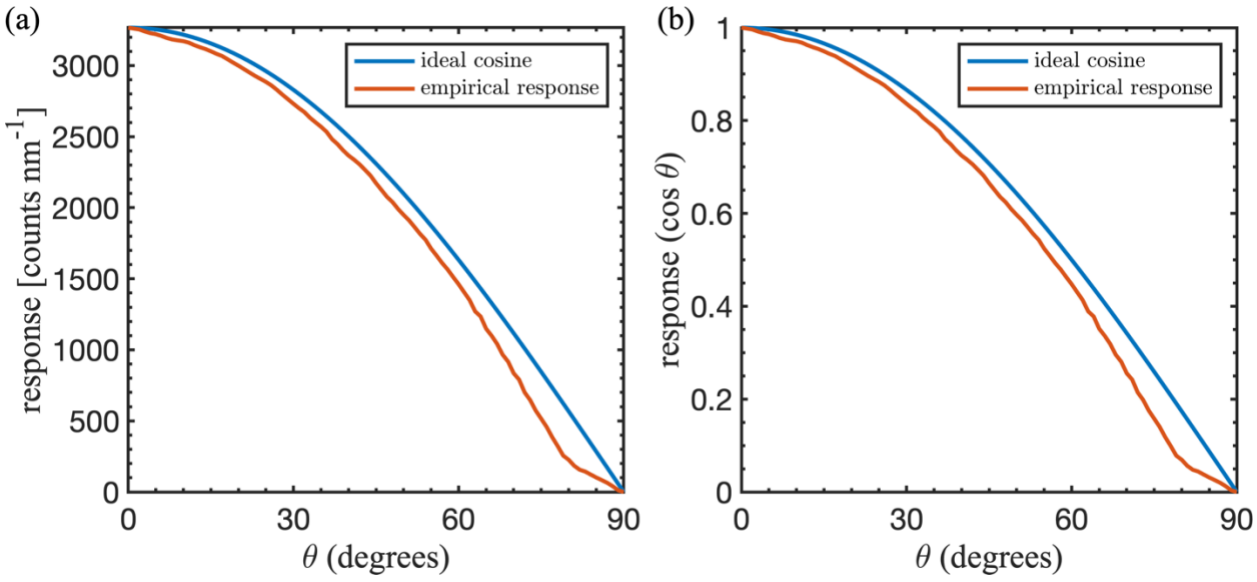

Fig. 6: (a) Comparison of ideal angular response function (ideal cosine) with the empirical angular response function used to estimate the non-ideal response of the irradiance sensor used in this study. The empirical angular response function was developed by Ocean Optics from laboratory measurements on the same irradiance sensor type used in this study. (b) Same as (a) but normalized. The red line in (b) is the empirical probability density function used as the irradiance source function for our backward-Monte Carlo simulations (see Eq. 21–22).

S1.2.2 Scattering and absorption by detector rod

If a photon trajectory crosses the 3-dimensional position of the detector rod, the photon energy density is reduced by an amount $1 - \omega_{\mathrm{rod}}$ and the photon is scattered away from the rod (Fig. 5) with an isotropic scattering phase function:

$$\theta_s = 1 - 2q, \tag{23}$$

$$\phi_s = 2\pi q. \tag{24}$$

The collision point is determined with ray tracing formulas that equate the vector equation of the photon trajectory with the parametric equation for the cylindrical detector rod surface following Ertürk and Howell (2017) Sect. 7.1 Eq. 59–66.

The polyvinyl chloride (PVC) detector rod albedo ω_{rod} is estimated from values for the complex refractive index of PVC (Zhang et al., 2020). Let $\mu = \cos\theta$ be the cosine zenith angle of incident radiation with $\mu = +1$ vertically downward. Following Modest (2013) Section 2.5 Eq. 2.89–2.98, the Fresnel reflectivity and transmissivity to incident (downward) radiation are:

$$R_{\mathrm{F}}(\mu) = \frac{1}{2}\left[\left(\frac{\mu - \mathrm{n}\mu_{\mathrm{n}}}{\mu + \mathrm{n}\mu_{\mathrm{n}}}\right)^2 + \left(\frac{\mathrm{n}\mu - \mu_{\mathrm{n}}}{\mathrm{n}\mu + \mu_{\mathrm{n}}}\right)^2\right] \tag{25}$$

$$T_{\mathrm{F}}(\mu) = 1 - R_{\mathrm{F}}(\mu) \tag{26}$$

where $\mathrm{n} + \mathrm{ik}$ and $\mathrm{n}_0 + \mathrm{ik}_0$ are the complex refractive indices of PVC and air, respectively, and:

$$\mu_n = \sqrt{1 - (1 - \mu^2)/n^2} \tag{27}$$

is the refracted cosine zenith angle in the PVC pipe. Radiation transmitted into the PVC is attenuated exponentially:

$$a(\mu_n) = e^{-\tau/\mu_n} \tag{28}$$

where:

$$\tau = 4\pi kL/\lambda \tag{29}$$

is the optical thickness of the PVC pipe with wall thickness $L = 0.004$ m. Radiation that transmits through L is internally reflected upward from the inner wall in the direction μ_n and attenuated exponentially along path length τ. Radiation that reaches the outer wall at $\mu_n < \mu_c$ is transmitted across the outer wall according to $T_F(\mu_n)$ and reflected back into the PVC according to $R_F(\mu_n)$, where μ_c is the critical angle given by Snell's law:

$$\mu_c = \sqrt{1 - 1/n^2}. \tag{30}$$

Formulas for $T_F(\mu_n)$ and $R_F(\mu_n)$ are similar to Eq. 25 and Eq. 26 with modifications for total internal reflection about μ_c and are given elsewhere (Briegleb and Light, 2007; Liou, 2002).

The total reflectivity is estimated with the successive-order-of-scattering method (van de Hulst, 1980), which accounts for the multiple internal reflections and absorption within the PVC described by Eq. 25–30. We model the PVC pipe as a plane, which is justified because the radius of curvature is much larger than all wavelengths of light considered here. For the geometry and optical properties of the detector rod, the total reflectivity has the closed-form solution:

$$R_d = R_{F,\mu} + \frac{T_{F,\mu} R_{F,\mu_n} T_{F,\mu_n} a_{\mu_n}^2}{1 - R_{F,\mu_n} a_{\mu_n}^2} \tag{31}$$

where the subscripts μ and μ_n on R, T, and a indicate the direction of incident radiance.

S2 Model validation

The Monte Carlo model described above is verified by comparison with benchmark values for total diffuse reflectance R_d [W m^{-2}], total transmittance T_t [W m^{-2}], diffuse angular reflectance $R_d(\alpha)$ [W sr^{-1}] and diffuse angular transmittance $T_d(\alpha)$ [W sr^{-1}] tabulated by van de Hulst (1980). The angular quantities, which have units of radiant intensity, are defined with respect to the exiting angle normal to the surface α [rad]. For a plane-parallel slab with optical properties $\sigma_s = 0.9$ m^{-1}, $\sigma_a = 0.1$ m^{-1}, $g = 0.75$, and optical thickness $\tau = 2$, the van de Hulst (1980) solutions are $R_d = 0.09739$ and $T_t = 0.66096$. For an ensemble of $N = 100$ simulations, the Monte Carlo model described above gives $R_d = 0.09740 \pm 0.00034$ and $T_t =$

0.66098 ± 0.00049 ($\mu \pm 1\sigma$). The model closely reproduces the benchmark solutions for $R_{\mathrm{d}}(\alpha)$ and $T_{\mathrm{d}}(\alpha)$ (Fig. 7).

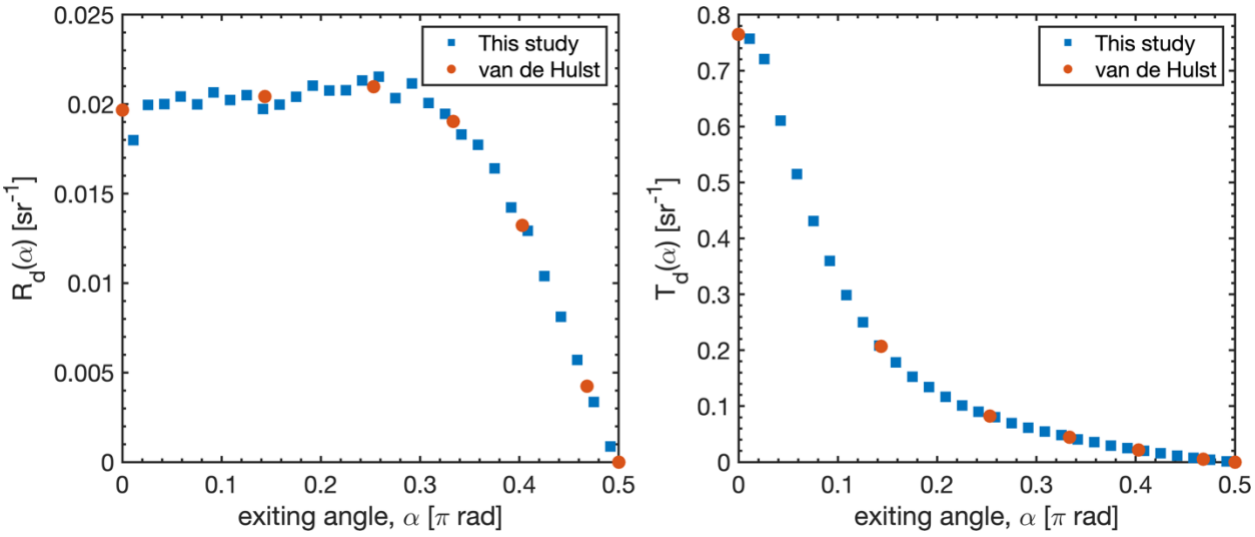

Fig. 7: Values of diffuse angular reflectance (radiant intensity), $R_d(\alpha)$ and transmittance $T_d(\alpha)$ vs. the photon exiting angle with respect to the surface normal α (after Wang et al. 1995 Fig. 3). Solid circles are benchmark solutions from Table 35 in van de Hulst (1980), obtained with the doubling method of solution to the radiative transfer equation.

S3 Monte Carlo uncertainty estimate

The Monte Carlo model is used to estimate the effect of detector interference on our irradiance measurements and, in turn, the asymptotic flux attenuation coefficients k_{att} that are estimated from them. To this end, we designed four experiments that isolate two forms of detector interference: 1) the non-ideal cosine response of the irradiance detector, and 2) absorption and scattering by the PVC detector rod. The four experiments, including a base simulation with no detector interference, are summarized in Table S1.

Table S1: Summary of four Monte Carlo experiments that simulate the effect of the detector rod interference on in-ice irradiance measurements. The baseline simulation (ideal diffusion, no rod) has no detector interference.

Experiment	Source function	Detector absorption	Detector scattering
Ideal Diffusion, No Rod	Eq. 23-24	-	-
Ideal Cosine, No Rod	Eq. 22	-	-
Ideal Cosine, With Rod	Eq. 22	ω_{rod}	Eq. 23-24
Non-ideal Cosine, With Rod	Empirical (Fig. 6)	ω_{rod}	Eq. 23-24

For each experimental setup, the Monte Carlo is integrated across 10,000 interactions at four wavelengths (400 nm, 500 nm, 600 nm, and 700 nm) with detector rod positions that are identical to the measurement depths reported in this paper (c.f. Fig. 5). For the 20 July experiment, these depths are 9.35 cm, 30.0 cm,

50.45 cm, and 68.60 cm, in units of solid-ice equivalent (i.e., physical thickness scaled by measured ice density). For the 21 July experiment, these depths are 45.93 cm, 58.98 cm, 73.40 cm, and 114.5 cm. Monte Carlo k_{att} values are estimated for each wavelength with the same method used for the field-estimates, i.e., by least-squares linear regression:

$$-\log T(\mathrm{z},\lambda) = T_0 + k_{\mathrm{att}}(\lambda)\mathrm{z} + \varepsilon \tag{32}$$

where T is the total diffuse transmittance from Monte Carlo simulation (see Section S2), T_0 is a parameter (y-intercept) that represents $T(\mathrm{z}=0)$ and ε is an error term.

These simulations provide two measures of k_{att} uncertainty: 1) the difference between the average Monte Carlo k_{att} value μ_{MC} and the field-estimated k_{att} value at each wavelength, and 2) the spread among Monte Carlo k_{att} values at each wavelength. The spread among Monte Carlo k_{att} values is an estimate of uncertainty due to the irradiance sensor angular response function and the detector rod interference. The spectrometer dark-light sensitivity is an additional source of instrumental uncertainty that is estimated from field measurements as described in Sect. X. These instrumental uncertainties (irradiance sensor angular response, detector rod interference, and dark-light sensitivity) are compared with the statistical variations in the high-frequency irradiance measurements and with the statistical uncertainty in the k_{att} linear regression model (Eq. 32).

If we take the spread among the Monte Carlo k_{att} values as independent of the uncertainty estimates obtained from analysis of field datasets and the uncertainty in the linear regression model, a combined uncertainty is estimated as:

$$\varepsilon = \sqrt{\varepsilon_{MC}^2 + \varepsilon_D^2 + \varepsilon_{2\sigma}^2 + \varepsilon_{LM}^2} \tag{33}$$

where ε_{MC}, ε_D, $\varepsilon_{2\sigma}$, and ε_{LM} are the uncertainty from Monte Carlo, dark-current sensitivity, high-frequency statistical variability, and linear model statistical uncertainty, defined as one standard error in the k_{att} linear regression (Fig 8).

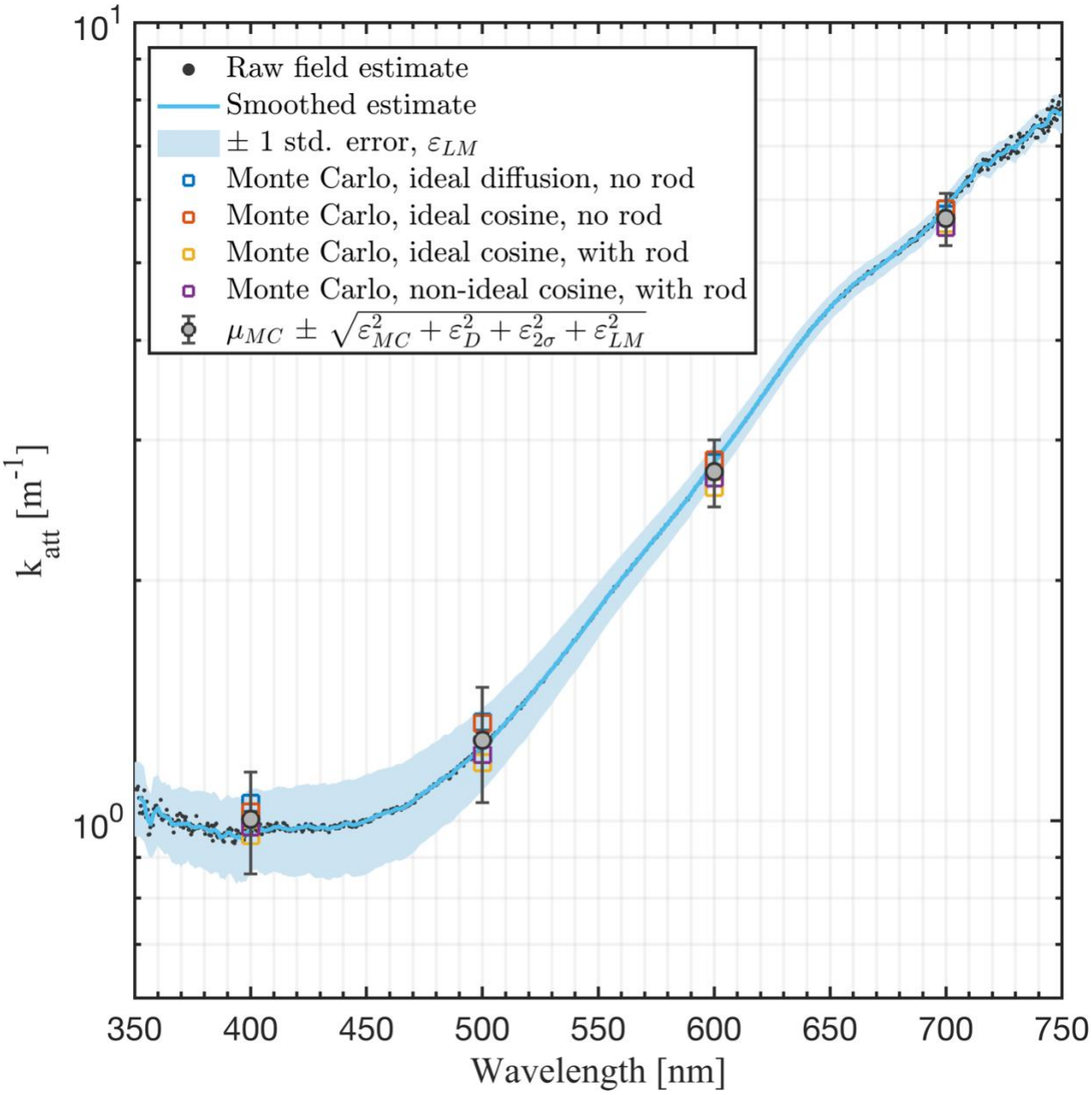

Fig 8: Attenuation coefficient k_{att} spectra from measurements of light transmission collected on 20 July, 2018, compared with average k_{att} values from four simulations with a 3-dimensional Monte Carlo radiative transfer model (μ_{MC}) and with two measures of uncertainty: 1) statistical linear model uncertainty ε_{LM} (shaded uncertainty bounds; ± 1 standard error in the linear regression) and, 2) ε_{LM} combined with instrumental and measurement uncertainty (error bars; $\mu_{MC} \pm \varepsilon$). The combined estimate combines ε_{LM} with uncertainty due to spectrometer dark-light sensitivity, non-ideal cosine response of the irradiance sensor, detector rod interference, and statistical variations in the high-frequency raw data (± 2 standard deviations).

References

Briegleb, B. P. and Light, B.: A Delta-Eddington Mutiple Scattering Parameterization for Solar Radiation in the Sea Ice Component of the Community Climate System Model, Technical Note, National Center for Atmospheric Research, Boulder, Colorado. [online] Available from: http://dx.doi.org/10.5065/D6B27S71 (Accessed 18 February 2019), 2007.

Ertürk, H. and Howell, J. R.: Monte Carlo Methods for Radiative Transfer, in Handbook of Thermal Science and Engineering, edited by F. A. Kulacki, pp. 1–43, Springer International Publishing, Cham., 2017.

Gordon, H. R.: Ship perturbation of irradiance measurements at sea 1: Monte Carlo simulations, Appl. Opt., 24(23), 4172, doi:10.1364/AO.24.004172, 1985.

van de Hulst, H. C.: Multiple light scattering: tables, formulas, and applications, Academic Press, New York., 1980.

Leathers, R. A., Downes, T. V., Davis, C. O. and Mobley, C. D.: Monte Carlo Radiative Transfer Simulations for Ocean Optics: A Practical Guide, Memorandum, Naval Research Laboratory, Washington, D.C. [online] Available from: https://www.oceanopticsbook.info/packages/iws_l2h/conversion/files/Leathersetal_NRL2004.pdf (Accessed 11 October 2020), 2004.

Light, B., Maykut, G. A. and Grenfell, T. C.: A two-dimensional Monte Carlo model of radiative transfer in sea ice, J. Geophys. Res. Oceans, 108(C7), 3219, doi:10.1029/2002JC001513, 2003.

Liou, K.-N.: An introduction to atmospheric radiation, 2nd ed., Academic Press, Amsterdam ; Boston., 2002.

Modest, M. F.: Radiative heat transfer, Third Edition., Academic Press, New York., 2013.

Mullen, P. C. and Warren, S. G.: Theory of the optical properties of lake ice, J. Geophys. Res. Atmospheres, 93(D7), 8403–8414, doi:10.1029/JD093iD07p08403, 1988.

Wang, L., Jacques, S. L. and Zheng, L.: MCML—Monte Carlo modeling of light transport in multi-layered tissues, Comput. Methods Programs Biomed., 47(2), 131–146, doi:10.1016/0169-2607(95)01640-F, 1995.

Zhang, X., Qiu, J., Li, X., Zhao, J. and Liu, L.: Complex refractive indices measurements of polymers in visible and near-infrared bands, Appl. Opt., 59(8), 2337, doi:10.1364/AO.383831, 2020.